

## Transferable Potentials for Phase Equilibria. 6. United-Atom Description for Ethers, Glycols, Ketones, and Aldehydes

John M. Stubbs,<sup>†</sup> Jeffrey J. Potoff,<sup>†,‡</sup> and J. Ilja Siepmann<sup>\*,†</sup>

*Departments of Chemistry and of Chemical Engineering and Material Science, University of Minnesota, 207 Pleasant Street SE, Minneapolis, Minnesota 55455-0431, Department of Chemical Engineering and Materials Science, Wayne State University, 5050 Anthony Wayne Drive, Detroit, Michigan 48202-3902*

*Received: February 5, 2004; In Final Form: August 12, 2004*

The extension of the transferable potentials for phase equilibria–united atom (TraPPE–UA) force field to the ether, glycol, ketone, and aldehyde functionalities is presented. New parameters for the ether oxygen, the carbonyl carbon (ketones), the carbonyl methine (aldehydes), and a special intramolecular hydrogen-bond term were fitted to the vapor–liquid coexistence curves for selected one-component systems. Coupled–decoupled configurational bias Monte Carlo simulations in the Gibbs or grand canonical ensemble were used to compute the vapor–liquid coexistence curves for the neat systems of dimethyl ether, ethyl methyl ether, diethyl ether, dipropyl ether, diisopropyl ether, methyl *tert*-butyl ether, 1,2-ethanediol, 2-methoxyethan-1-ol, 1,2-dimethoxyethane, 1,3-propanediol, acetone, 2-pentanone, 2-octanone, acetaldehyde, pentanal, and octanal. Additional simulations were performed for the binary mixtures of diethyl ether + ethanol and acetone + hexane. Excellent agreement with experimental results was found with the mean unsigned errors being less than 1% for the critical temperatures and about 3% (ethers) and 1% (other) for the normal boiling temperatures. For the mixture of acetone + hexane at 328.15 K, a positive pressure azeotrope was found with  $x_{\text{acetone}}^{\text{azeo}} = 0.71$  in satisfactory agreement with the experimental result of 0.64. Additionally, the structures of hydrogen-bonded aggregates were investigated for 1,2-ethanediol and 2-methoxyethan-1-ol, where the average hydrogen-bond energies were found to be about  $-20$  and  $-14$  kJ mol<sup>-1</sup> for inter- and intramolecular hydrogen bonds, respectively.

### I. Introduction

There is considerable interest in the thermophysical properties of molecules containing ether, ether + alcohol (glycol), and carbonyl functionalities both as pure solvents and solvent mixtures. In particular, aliphatic ethers and polyethers find use as gasoline additives, are present in chromatographic stationary phases, are common in nonionic surfactants, and additionally, are employed as cosolvents in supercritical fluids. Despite this importance, experimental data exists primarily only for low molecular weight compounds or for larger compounds only at low temperatures due to thermal decomposition. Molecular simulations using empirical force fields can circumvent this problem and determine physical properties for larger compounds at elevated temperatures, but with an accuracy limited by the force field employed.

The united-atom OPLS (optimized potentials for liquid simulations) force field developed by Jorgensen and co-workers for dimethyl, ethyl methyl, and diethyl ether<sup>1</sup> and acetone<sup>2</sup> optimizes parameters to reproduce thermodynamic quantities at or near standard temperature and pressure. For conditions further away from this point, for example, near the critical point, the OPLS models become less robust. Starting with a generalized force field for *n*-alkanes,<sup>3</sup> it has been an ongoing goal of this research group to create a transferable, computationally efficient force field for general use in simulations. Called TraPPE (transferable potentials for phase equilibria), this force field has

already found varying applications, ranging from retention in chromatographic systems,<sup>4,5</sup> octanol–water partitioning,<sup>6</sup> dynamics in biophysical systems,<sup>7</sup> design of biomimetic polymers,<sup>8</sup> miscibility in polymer systems,<sup>9</sup> adsorption in pharmaceutical solids,<sup>10</sup> and transport properties of lubricants.<sup>11–13</sup> Presented here is the extension of the united-atom version of the TraPPE force field, TraPPE–UA, to molecules containing ether, glycol, diol, ketone, or aldehyde functionalities, where it was necessary to develop parameters for ether –O–, ketone C (sp<sup>2</sup>), and aldehyde methine (sp<sup>2</sup>) sites. In the united-atom formalism, all hydrogen atoms that are bonded to carbon atoms are treated as a single interaction site, for example, a methyl group becomes a single pseudo-atom, CH<sub>3</sub>. No additional sites needed to be determined for ethers, glycols, ketones, and aldehydes because these three new sites were fit by transferring parameters for CH<sub>3</sub>, CH<sub>2</sub>, CH, C, hydroxyl oxygen and hydrogen, and carbonyl oxygen from earlier works.<sup>3,14–16</sup> It was found that the addition of full intramolecular charge interactions for sites separated by four or more bonds and that scaled interactions for sites separated by three bonds allowed multifunctional molecules to be successfully modeled with no further optimization of the bonded and nonbonded parameters for the sites involved, for example, 1,3-propanediol was determined to have a boiling point that deviated from experiment by only 0.6%.

### II. Model

The TraPPE–UA force field employs pseudo-atoms representing all CH<sub>*x*</sub> groups (with 0 ≤ *x* ≤ 4) that are located at the position of the carbon atom. The nonbonded interactions are

\* Corresponding author. E-mail: siepmann@chem.umn.edu.

<sup>†</sup> University of Minnesota.

<sup>‡</sup> Wayne State University.

composed of pairwise additive Lennard-Jones (LJ) and Coulombic potentials

$$u(r_{ij}) = 4\epsilon_{ij} \left[ \left( \frac{\sigma_{ij}}{r_{ij}} \right)^{12} - \left( \frac{\sigma_{ij}}{r_{ij}} \right)^6 \right] + \frac{q_i q_j}{4\pi\epsilon_0 r_{ij}} \quad (1)$$

where  $r_{ij}$ ,  $\epsilon_{ij}$ ,  $\sigma_{ij}$ ,  $q_i$ , and  $q_j$  are the bead–bead separation, the LJ well depth, the LJ diameter, and the partial charges on beads  $i$  and  $j$ , respectively. The unlike interactions are computed with the Lorentz–Berthelot combining rules<sup>17,18</sup>

$$\sigma_{ij} = \frac{1}{2}(\sigma_{ii} + \sigma_{jj}) \quad \epsilon_{ij} = \sqrt{\epsilon_{ii}\epsilon_{jj}} \quad (2)$$

Here we emphasize that a CH<sub>x</sub> pseudo-atom represents not only the interactions of the valence electrons constituting its  $x$  C–H bonds but also a share of the valence electrons constituting the  $4 - x$  C–C bonds (for sp<sup>3</sup> carbons). Thus, the Lennard-Jones parameters need to reflect both of these contributions. Furthermore, C–H bonds are relatively short compared to C–C or C–O bonds. Together, this gives a plausible explanation as to why the TraPPE–UA Lennard-Jones diameters of the CH<sub>x</sub> pseudo-atoms are found to increase with decreasing  $x$ .<sup>3,14,19</sup>

As previously implemented in the TraPPE–UA force field,<sup>3,14,15,20</sup> nonbonded interactions are calculated for intermolecular interactions and for intramolecular interactions of beads separated by four or more bonds. Intramolecular Coulombic interactions separated by three bonds were reduced in magnitude by a scaling factor of  $1/2$ , as implemented in earlier versions of the AMBER force field.<sup>21,22</sup> Additionally, initial simulations of glycol ethers showed the necessity of a short-range repulsive term for intramolecular interactions of a hydroxyl hydrogen (that is not protected by a LJ potential) and an oxygen atom separated by four bonds, and the following simple form is used

$$u_{\text{repulsive}}(r_{ij}) = \frac{a_x}{r_{ij}^{12}} \quad (3)$$

with  $a_{\text{ether}} = 4.0 \times 10^7 \text{ K } \text{\AA}^{12}$  and  $a_{\text{alcohol}} = 7.5 \times 10^7 \text{ K } \text{\AA}^{12}$  for an intramolecular hydrogen bond with a neighboring ether oxygen and alcohol oxygen, respectively.

Rigid bond lengths are used for bonded 1–2 interactions. Beads separated by two bonds interact via a harmonic bending potential

$$u_{\text{bend}} = \frac{k_{\theta}}{2}(\theta - \theta_{\text{eq}})^2 \quad (4)$$

where  $k_{\theta}$ ,  $\theta$ , and  $\theta_{\text{eq}}$  are the force constant, the bending angle, and the equilibrium bending angle, respectively. A cosine series is employed for torsional interactions of beads separated by three bonds

$$u_{\text{tors}} = c_0 + c_1[1 + \cos(\phi)] + c_2[1 - \cos(2\phi)] + c_3[1 + \cos(3\phi)] \quad (5)$$

where  $\phi$  and  $c_i$  are the dihedral angle and the  $i$ th coefficient, respectively. Tables 1 and 2 list the values of the TraPPE–UA ether, glycol ether, ketone, and aldehyde bonded and nonbonded force field parameters, respectively.

**A. Ether Model.** For the ether model, the transferability of the TraPPE force field was exploited to create most of the parameters that were needed. All LJ parameters for carbon pseudo-atoms were taken from the TraPPE–UA alcohol force

**TABLE 1: TraPPE–UA Force-Field Parameters for Bonded Interactions**

bond length	molecule	$r_0$ (Å)		
CH <sub>x</sub> –CH <sub>y</sub>	all	1.54		
CH <sub>x</sub> –O	ether	1.41		
C=O	ketone	1.229		
CH=O	aldehyde	1.217		
CH <sub>x</sub> –C	aldehyde/ketone	1.52		
bend (eq 4)	$\theta_0$ (deg)	$k_{\theta}/k_B$ (K)		
CH <sub>x</sub> –CH <sub>2</sub> –CH <sub>y</sub>	114	62 500		
CH <sub>x</sub> –CH–CH <sub>y</sub>	112	62 500		
CH <sub>x</sub> –C–CH <sub>y</sub>	109.47	62 500		
CH <sub>x</sub> –CH <sub>y</sub> –O	112	50 300		
CH <sub>x</sub> –O–CH <sub>y</sub>	112	60 400		
CH <sub>x</sub> –C(=O)–CH <sub>y</sub>	117.2	62 500		
CH <sub>x</sub> –C=O	121.4	62 500		
torsion (eq 5)	$c_0/k_B$ (K)	$c_1/k_B$ (K)	$c_2/k_B$ (K)	$c_3/k_B$ (K)
CH <sub>x</sub> –CH <sub>2</sub> –CH <sub>2</sub> –CH <sub>y</sub>	0	335.03	−68.19	791.32
CH <sub>x</sub> –CH <sub>y</sub> –O–CH <sub>z</sub>	0	725.35	−163.75	558.20
CH <sub>x</sub> –CH <sub>2</sub> –CH <sub>2</sub> –O	0	176.62	−53.34	769.93
O–CH <sub>2</sub> –CH <sub>2</sub> –O	503.24	0	−251.62	1006.47
CH <sub>x</sub> –CH <sub>2</sub> –C=O	2035.58	−736.90	57.84	−293.23

**TABLE 2: TraPPE–UA Force-Field Parameters for Nonbonded Interactions**

site	molecule	$\sigma$ (Å)	$\epsilon/k_B$ (K)	$q$ (e)
CH <sub>3</sub> (sp <sup>3</sup> )	ether/alcohol/aldehyde	3.75	98.0	+0.25 <sup>a</sup> /+0.265 <sup>b</sup> /–0.043 <sup>c</sup>
CH <sub>2</sub> (sp <sup>3</sup> )	ether/alcohol/aldehyde	3.95	46.0	+0.25 <sup>a</sup> /+0.265 <sup>b</sup> /–0.043 <sup>c</sup>
CH(sp <sup>3</sup> )	ether/alcohol	4.33	10.0	+0.25 <sup>a</sup> /+0.265 <sup>b</sup>
C(sp <sup>3</sup> )	ether/alcohol	5.80	0.5	+0.25 <sup>a</sup> /+0.265 <sup>b</sup>
CH <sub>3</sub> (sp <sup>3</sup> )	all other	3.75	98.0	0
CH <sub>2</sub> (sp <sup>3</sup> )	all other	3.95	46.0	0
CH(sp <sup>3</sup> )	all other/aldehyde	4.68	10.0	0/–0.043 <sup>c</sup>
C(sp <sup>3</sup> )	all other/aldehyde	6.40	0.5	0/–0.043 <sup>c</sup>
O	ether	2.80	55.0	–0.500
O	alcohol	3.02	93.0	–0.700
H	alcohol			+0.435
CH(sp <sup>2</sup> )	aldehyde	3.52	54.0	+0.525
O(sp <sup>2</sup> )	aldehyde	3.05	79.0	–0.482
C(sp <sup>2</sup> )	ketone	3.82	40.0	+0.424
O(sp <sup>2</sup> )	ketone	3.05	79.0	–0.424

<sup>a</sup> For sites adjacent to the ether oxygen. <sup>b</sup> For sites adjacent to the alcohol oxygen. <sup>c</sup> For sites adjacent to the aldehyde carbon.

field<sup>15</sup> as were the C–C–C–O torsional potential and any terms that did not involve the oxygen site, for example, carbon–carbon bond length. The OPLS–UA force field<sup>1</sup> provided the partial charges, carbon–oxygen bond length, the C–C–O–C torsional potential, and the equilibrium C–C–O and C–O–C bending angles, whereas the bending force constants were taken from the AMBER94 force field<sup>23</sup> because they are treated as rigid in the OPLS–UA model. The new TraPPE  $\sigma$  and  $\epsilon$  parameters for the ether oxygen were obtained from simultaneous fits to the vapor–liquid coexistence curves of dimethyl ether, ethyl methyl ether, and diethyl ether.

**B. Glycol Model.** With an ether and alcohol<sup>15</sup> model in place, the combination of the two allows for the construction of a force field for (R–[–CH<sub>2</sub>–CH<sub>2</sub>–O–]<sub>*n*</sub>–R') with R and R' being both hydroxyl groups (poly(ethylene glycol)), both alkyl groups (poly(ethylene oxide)), or one of each by the addition of an O–C–C–O torsional potential and formalism for neighboring intramolecular charge groups to interact. The choice of the O–CH<sub>2</sub>–CH<sub>2</sub>–O torsional potential from the AMBER 94 force field<sup>23</sup> coupled with scaling of 1–4 charge interactions by a factor of  $1/2$  and optimization of intramolecular 1–5 hydroxyl hydrogen–oxygen repulsive terms, one for two hydroxyl groups, and one for a hydroxyl and ether combination produced

satisfactory results for the test cases of 1,2-ethanediol, 2-methoxyethan-1-ol, and 1,2-dimethoxyethane.

**C. Aldehyde and Ketone Models.** As in the case of previous extensions of the TraPPE force field, we exploited transferability to reduce the number of new parameters that required fitting. The Lennard-Jones parameters for CH<sub>3</sub> and CH<sub>2</sub> pseudo-atoms were taken from the TraPPE-UA force field for alkanes.<sup>3</sup> The Lennard-Jones parameters for the carbonyl oxygen were taken from the TraPPE force field for CO<sub>2</sub>.<sup>16</sup> Partial charges for the ketone carbonyl oxygen and carbon were taken from the OPLS-UA force field.<sup>2</sup> Partial charges for the aldehyde functionality were derived from the CHELPG<sup>24</sup> fit to the ab initio potential-energy surface generated with Gaussian 98<sup>25</sup> at the MP2/6-31 g(d,p) level of theory because initial tests with the OPLS-UA charges would not allow for satisfactory agreement with experimental data for boiling points and critical temperatures. As a result, the only parameters that required fitting were  $\epsilon$  and  $\sigma$  for the carbonyl carbon in ketones and the CH group in aldehydes. These parameters were tuned until the vapor-liquid coexistence curves for acetaldehyde and acetone predicted by simulation were in good agreement with experimental data.

### III. Simulation Details

The Gibbs ensemble Monte Carlo<sup>26-28</sup> (GEMC) and histogram-reweighting grand canonical Monte Carlo (GCMC-HR) techniques<sup>29-31</sup> were used in conjunction with the coupled-decoupled configurational-bias Monte Carlo<sup>14,32-36</sup> (CBMC) method to determine the saturated vapor-liquid densities for one component systems and binary vapor-liquid coexistence curves (VLCC). Additionally, self-adapting fixed-endpoint configurational bias Monte Carlo<sup>37</sup> (SAFE-CBMC) moves were employed for longer polyethers to sample their interior conformational degrees of freedom accurately. An Ewald summation technique, with  $\kappa \times L = 5$ ,  $K_{\max} = 5$ , and tin foil boundary conditions, was used in the calculation of the long-range electrostatic interactions.<sup>38</sup> The normal boiling points ( $T_b$ ) were calculated via the Clausius-Clapeyron equation. For GEMC simulations, the critical temperatures ( $T_c$ ) and densities ( $\rho_c$ ) were calculated using the saturated density scaling law and the law of rectilinear diameters with a scaling exponent of  $\beta^* = 0.325$ .<sup>41,42</sup> For GCMC simulations, the critical points were determined from a mixed-field matching analysis.<sup>39,40</sup> Given the simplicity of the TraPPE-UA force field, finite size effects on the critical properties were not explored.

**A. Gibbs Ensemble Monte Carlo Simulations.** The system sizes for the calculations of the saturated vapor-liquid coexistence curves in the  $NVT$  and  $NpT$  Gibbs ensemble were 300 molecules for pure ethers and the diethyl ether/ethanol mixture and 250 molecules for glycols, with a nonbonded potential cutoff of 14 Å for the pure component and 12 Å for the binary system, beyond which analytic tail corrections were employed for the LJ interactions.<sup>38,43</sup> At least 25 000 and 50 000 cycles were used for equilibration and production periods, respectively, where one cycle consists of an  $N_{\text{molecules}}$  number of Monte Carlo steps.

**B. Grand Canonical Monte Carlo Simulations.** Coupled-decoupled configurational bias Monte Carlo simulations in the grand canonical ensemble were used to determine the vapor-liquid coexistence curves for pure aldehydes and ketones as well as a mixture of acetone and *n*-hexane. Histogram reweighting methods were used to construct the phase diagrams from the probability distributions that were extracted from the simulations. A box length of  $L = 30$  Å was used for simulations of acetaldehyde and acetone, whereas simulations of longer aldehydes and ketones were performed for  $L = 35$  Å. Lennard-

Jones interactions were truncated at 10 Å, and analytical tail corrections were applied. Equilibration periods consisted of more than 10<sup>6</sup> Monte Carlo Steps (MCS). Vapor-phase simulations were run for 10<sup>7</sup> MCS, whereas simulations performed in the liquid phase were run for  $2 \times 10^7$  MCS. Simulation data were stored in the form of lists containing the number of molecules and the energy of the system. Samples were written to these lists every 250 MCS.

**C. Comparison of Gibbs Ensemble and Grand Canonical Monte Carlo Approaches.** Both GEMC and GCMC-HR approaches employed here offer specific advantages for phase equilibrium calculations. In our opinion, neither approach is clearly superior for the systems investigated here. The main advantages of the GEMC method are its ease of use (at least for pure systems, requiring very little human input throughout the simulation) and trivial parallelization; that is, a separate simulation for each state point can be submitted to a given processor, thereby allowing all state points to run in parallel on multiple processors. GEMC's main disadvantage is that the determination of the critical point requires an extrapolation procedure of near-critical coexistence data. The main advantage of the GCMC-HR is that it allows for a more precise determination of the critical point using a mixed-field finite-size scaling analysis for both pure systems and mixtures.<sup>31</sup> The main disadvantage of GCMC-HR is that it has a substantial need for human input throughout the multiple simulations required to obtain a complete VLCC.

Beyond these general points, there are some specific considerations for the systems studied here. Using relatively simple force fields with their underlying approximations (e.g., Lennard-Jones potential, fixed charges, and united atom representation), it appears that the precision of GEMC data is more than sufficient to point to limits of the accuracy of the force field. Although GCMC-HR is more efficient for simple molecules for which only conventional particle translations and swaps are required,<sup>31</sup> the systems studied here require the extensive use of CBMC techniques. For GEMC particle swap moves, split-energy techniques<sup>36</sup> (i.e., a significantly shorter spherical potential truncation at 5 Å) can be used for the calculation of the Rosenbluth weights that result in substantial computer time savings. In contrast, the CBMC particle swap moves in the grand canonical ensemble require the use of the full potential throughout the calculation of the Rosenbluth weights, as do calculations of the chemical potential via particle insertion methods.

### IV. Results and Discussion

**A. Pure Component Vapor-Liquid-Phase Equilibria.** The pure component saturated vapor-liquid densities and saturated vapor pressures for the ether models tested are shown in Figures 1, 2, 3, and 4. There is excellent agreement with experiment; in particular, the deviation from the experimental saturated liquid density curve is comparable with the deviations from predictions of the Rackett equation for saturated liquid densities.<sup>44</sup>

Table 3 compares  $T_b$ ,  $T_c$ , and  $\rho_c$  for the TraPPE-UA and OPLS-UA ether models with the experimental values. For the TraPPE-UA model,  $T_c$  and  $\rho_c$  are in excellent agreement with experimental values,<sup>45,44</sup> whereas  $T_b$  is about 3% too low for all of the ethers (with the exception of the more polar 1,2-dimethoxyethane). This is consistent with previous results for the TraPPE-UA force field<sup>3,14,20</sup> and is due in part to the use of TraPPE-UA parameters for carbon sites. Although the OPLS-UA model for dimethyl ether compares favorably with experiment, it deviates significantly for ethyl methyl ether and diethyl ether. Figures 5 and 6 illustrate these differences by

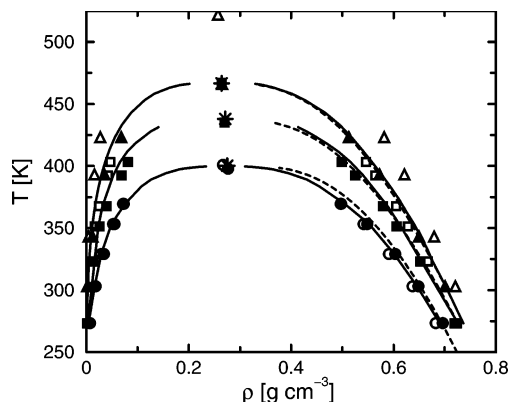


**Figure 1.** Vapor-liquid coexistence curves for dimethyl ether (circles), ethyl methyl ether (squares), and diethyl ether (triangles). Solid lines and stars depict the experimental coexistence densities and critical points.<sup>45</sup> The dashed lines show the Rackett correlation.<sup>44</sup> Filled and open symbols show the simulation results calculated for the TraPPE-UA and OPLS-UA force fields, respectively. Statistical uncertainties in the simulation data are smaller than the symbol size.

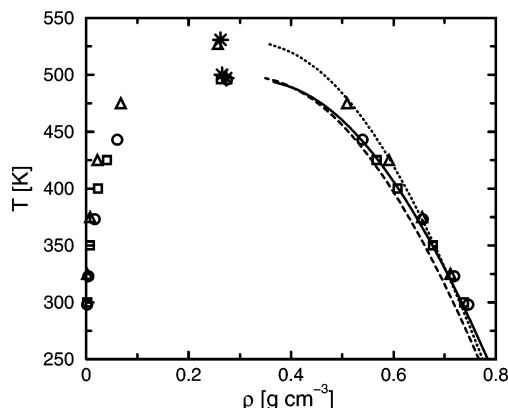


**Figure 2.** Vapor-liquid coexistence curves for methyl *tert*-butyl ether (solid line and circles), diisopropyl ether (dashed line and squares), and dipropyl ether (dotted line and triangles). Stars and lines depict the experimental critical points<sup>45</sup> and the Rackett correlation,<sup>44</sup> respectively. Circles, squares, and triangles show the simulation results for the TraPPE-UA force field.

comparing the calculated  $T_b$  and  $T_c$  values for the ether model with the experimental values. As can be seen in Figure 5, the TraPPE-UA normal boiling points for ethers are consistently shifted, whereas for the OPLS-UA model, the slope is different and the deviations increase with increasing molecular weight. The poor performance of the OPLS-UA model in predicting  $T_c$  is shown in Figure 6 where, in the case of diethyl ether, the value is overestimated by 12%. Given that no fitting of parameters beyond the first three ethers (dimethyl ether, ethyl methyl ether, and diethyl ether) was undertaken, the robustness of the TraPPE-UA model can be seen in the predictions of higher molecular weight ethers (including branched ethers that were not considered at all during the parameter development) such as methyl *tert*-butyl ether, diisopropyl ether, and dipropyl ether, whose critical temperatures all fall within 1% of the experimental values.

To include intramolecular charge interactions for the case of neighboring neutral charge groups (as opposed to the case of 1,5-pentanediol,<sup>15</sup> where there are no charged sites within three bonds of one another), we investigated several possible interaction rules. The final choice of scaling 1–4 charge interactions by  $1/2$  reflects not only agreement with experimental properties for molecules where additional parameters were simultaneously being optimized, as in the case of 2-methoxyethan-1-ol, but also

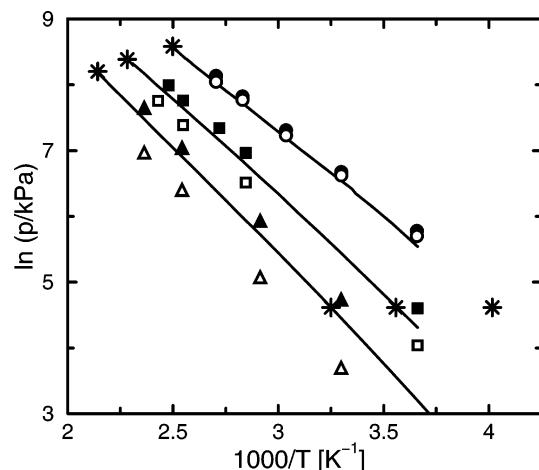


**Figure 3.** Clausius-Clapeyron plots of the saturated vapor pressure versus inverse temperature as predicted by the TraPPE-UA (filled symbols) and OPLS-UA (open symbols) force fields for dimethyl ether (circles), ethyl methyl ether (squares), and diethyl ether (triangles). Experimental saturated vapor pressure data<sup>45</sup> are shown as lines and the stars denote the experimentally determined critical points<sup>60</sup> and normal boiling points.<sup>59</sup>

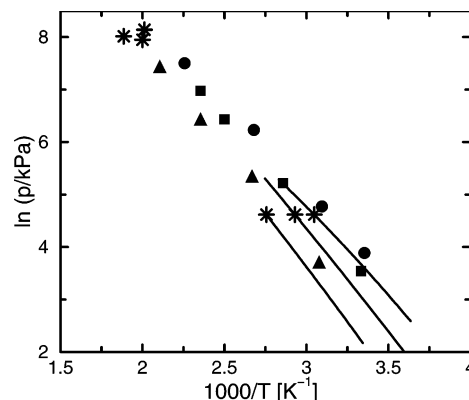


**Figure 4.** Clausius-Clapeyron plots of the saturated vapor pressure versus inverse temperature as predicted by the TraPPE-UA force field (filled symbols) for methyl *tert*-butyl ether (circles), diisopropyl ether (squares), and dipropyl ether (triangles). Correlation data<sup>44</sup> are shown as lines, and the stars denote the experimentally determined critical points<sup>60</sup> and normal boiling points.<sup>59</sup>

the very satisfactory reproduction of thermodynamic properties of several different molecules (Figures 7 and 8) where, because of model transferability, the only undefined parameter was the charge interaction rule. For example, excellent agreement with experiment is achieved for 1,3-propanediol where the boiling point is reproduced to within  $\sim 0.5\%$  and the liquid density at 350 K was reproduced to  $\sim 1\%$  of the experimental value.<sup>51</sup> The addition of a torsional potential for the O-CH<sub>2</sub>-CH<sub>2</sub>-O angle completed the model and allowed the simulation of 1,2-dimethoxyethane, where the boiling point of 359 K compares favorably to the experimental value of 358 K (Table 3), and additionally, the liquid density at 325 K is slightly overpredicted by  $\sim 1.5\%$  as compared to a correlation fit to experiment.<sup>46</sup> For comparison, simulations were also carried out for the all-atom force field for 1,2-dimethoxyethane developed by Smith et al.<sup>47,48</sup> with a nonbonded cutoff of 13 Å beyond which analytical tail corrections were used with an Ewald summation accounting for the long range electrostatic interactions. The resulting boiling and critical temperatures are 376 K and 569 K, respectively (i.e., both are overestimated by about 5%). Additionally, the density at 325 K is 0.842 g cm<sup>-3</sup>, overpredicted by  $\sim 1.3\%$ .<sup>46</sup> Although the two models give comparable results for the lower



**TABLE 3: Pure Component Properties for Ether and Glycols<sup>a</sup>**

molecule		$T_b$ (K)	$T_c$ (K)	$\rho_c$ (g cm <sup>-3</sup> )
dimethyl ether	TraPPE-UA	242 <sub>2</sub>	398 <sub>1</sub>	0.277 <sub>2</sub>
	OPLS-UA	244 <sub>1</sub>	401 <sub>1</sub>	0.267 <sub>1</sub>
	expt <sup>59,60</sup>	249 <sub>1</sub>	400.2 <sub>1</sub>	0.275 <sub>10</sub>
ethyl methyl ether	TraPPE-UA	272 <sub>1</sub>	435 <sub>1</sub>	0.270 <sub>2</sub>
	OPLS-UA	290 <sub>1</sub>	467 <sub>1</sub>	0.264 <sub>2</sub>
	expt <sup>59,60</sup>	280–283	437.9 <sub>1</sub>	0.271 <sub>5</sub>
diethyl ether	TraPPE-UA	297 <sub>1</sub>	466 <sub>2</sub>	0.265 <sub>3</sub>
	OPLS-UA	330 <sub>1</sub>	522 <sub>2</sub>	0.257 <sub>2</sub>
	expt <sup>59,60</sup>	307.7 <sub>2</sub>	466.7 <sub>1</sub>	0.264 <sub>3</sub>
methyl <i>tert</i> -butyl ether	TraPPE-UA	318 <sub>1</sub>	496 <sub>2</sub>	0.275 <sub>3</sub>
	expt <sup>59,60,44</sup>	328.2 <sub>2</sub>	497.1 <sub>2</sub>	0.273
diisopropyl ether	TraPPE-UA	331 <sub>1</sub>	496 <sub>2</sub>	0.263 <sub>3</sub>
	expt <sup>59,60</sup>	341.4 <sub>7</sub>	500.3 <sub>2</sub>	0.265 <sub>10</sub>
dipropyl ether	TraPPE-UA	352 <sub>1</sub>	527 <sub>1</sub>	0.257 <sub>2</sub>
	expt <sup>59,60,44</sup>	363 <sub>1</sub>	530.6 <sub>2</sub>	0.262
1,2-dimethoxyethane	TraPPE-UA	359 <sub>2</sub>	542 <sub>2</sub>	0.298 <sub>3</sub>
	Smith <sup>47,48</sup>	376 <sub>2</sub>	568 <sub>2</sub>	0.291 <sub>2</sub>
	expt <sup>59,60</sup>	358 <sub>1</sub>	540 <sub>3</sub>	0.293 <sub>20</sub>
1,2-ethanediol	TraPPE-UA	468 <sub>3</sub>	718 <sub>3</sub>	0.340 <sub>4</sub>
	expt <sup>59,60</sup>	470.5 <sub>5</sub>	720 <sub>10</sub>	
1,3-propanediol	TraPPE-UA	490 <sub>3</sub>	726 <sub>2</sub>	0.324 <sub>3</sub>
	expt <sup>59,60</sup>	487 <sub>3</sub>	722 <sub>5</sub>	
2-methoxyethan-1-ol	TraPPE-UA	391 <sub>2</sub>	590 <sub>2</sub>	0.321 <sub>3</sub>
	expt <sup>59,60</sup>	397.6 <sub>3</sub>	597.6 <sub>2</sub>	0.289 <sub>5</sub>

<sup>a</sup> Subscripts indicate uncertainties in the final digit.**TABLE 4: Pure Component Properties for Aldehyde and Ketones<sup>a</sup>**

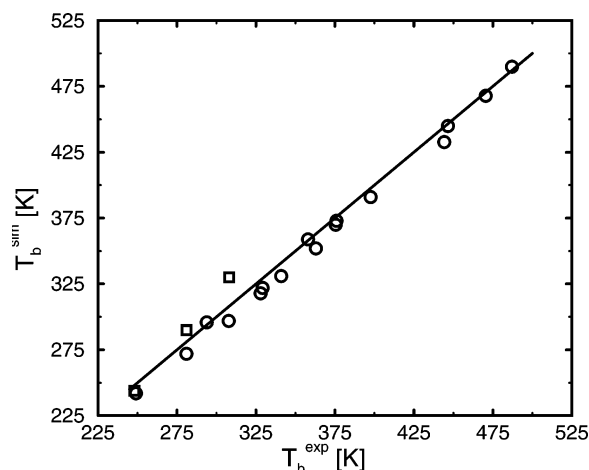
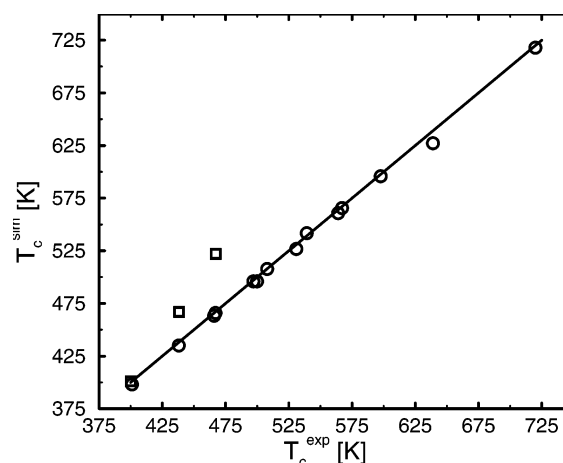
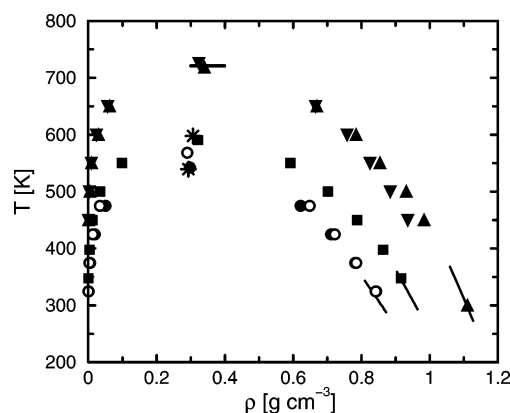
molecule		$T_b$ (K)	$T_c$ (K)	$\rho_c$ (g cm <sup>-3</sup> )
acetaldehyde	TraPPE-UA	295.9	463.4	0.2848
	expt <sup>59,60</sup>	293.9 <sub>8</sub>	466 <sub>2</sub>	0.286 <sub>5</sub>
pentanal	TraPPE-UA	373.1	565.8	0.2764
	expt <sup>59,60</sup>	376 <sub>2</sub>	567 <sub>2</sub>	0.275 <sub>5</sub>
octanal	TraPPE-UA	432.9	627.2	0.2744
	expt <sup>59,60</sup>	444.2	639 <sub>2</sub>	0.263 <sub>5</sub>
acetone	TraPPE-UA	322	508	0.278
	expt <sup>59,60</sup>	329.3 <sub>3</sub>	508.1 <sub>1</sub>	0.273 <sub>5</sub>
2-pentanone	TraPPE-UA	370	561	0.286
	expt <sup>59,60</sup>	375 <sub>1</sub>	561.1 <sub>2</sub>	0.268 <sub>5</sub>
2-octanone	TraPPE-UA	445	640	0.2517
	expt <sup>59,60</sup>	446 <sub>2</sub>	632.7 <sub>4</sub>	0.258 <sub>5</sub>

<sup>a</sup> Subscripts indicate uncertainties in the final digit.

temperature liquid densities, the vapor pressure is underpredicted by the all-atom model, which leads to the large deviations in  $T_b$  and  $T_c$  as compared to experiment (Figure 8).

The knowledge of the experimental boiling and critical temperatures of 1,2-ethanediol allowed for the optimization of the repulsive  $\alpha$  parameter (eq 3), which was the only interaction parameter not present in other test molecules. This resulted in a boiling point in excellent agreement with experimental data (Table 3). To investigate the performance of the model for larger polyether molecules, we computed the liquid density of triethylene glycol at two different state points: ( $T = 310$  K,  $p = 1$  bar) and (280 K, 20 bar). The resulting values of  $1.108 \pm 0.003$  and  $1.121 \pm 0.002$  g cm<sup>-3</sup> deviate by 0.2 and 1.2%, respectively, from experimental values of  $1.1107 \pm 0.0003$  and  $1.1350 \pm 0.0003$  g cm<sup>-3</sup>.<sup>49</sup>

The vapor–liquid coexistence curves for aldehydes and ketones are shown in Figures 9 and 10, respectively. Force-field parameters for aldehydes and ketones were determined from simulations of acetaldehyde and acetone, respectively. The corresponding  $\epsilon$  and  $\sigma$  parameters for C = (ketones) and CH = (aldehydes) were tuned to reproduce vapor–liquid coexistence curves and critical properties. Emphasis was placed on the

**Figure 5.** Scatter plot of the calculated normal boiling points versus the experimental values<sup>44,59,50</sup> for the 16 compounds listed in Tables 3 and 4. Circles and squares depict the results for the TraPPE-UA and OPLS-UA force fields, respectively.**Figure 6.** Scatter plot of the calculated critical temperatures versus the experimental values.<sup>44,59,60</sup> Symbols are the same as those in Figure 5.**Figure 7.** Vapor–liquid coexistence curves calculated for the TraPPE-UA (filled symbols) and Smith (open symbols) force fields for 1,2-dimethoxyethane (circles), 2-methoxyethan-1-ol (squares), 1,2-ethanediol (triangles up), and 1,3-propanediol (triangles down). Experimental saturated vapor pressure data<sup>46,50,51,59</sup> are shown as lines, and the stars denote the experimentally determined critical points<sup>60</sup> and normal boiling points.<sup>59</sup>

reproduction of saturated liquid densities in the force-field parametrization. These parameters were then used, without modification, for predicting the vapor–liquid coexistence curves of pentanal, octanal, 2-pentanone, and 2-octanone. In all cases,

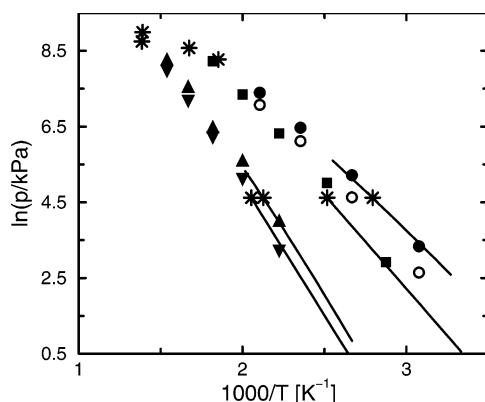


**Figure 8.** Clausius–Clapeyron plots of the saturated vapor pressure versus inverse temperature calculated for the TraPPE–UA (filled symbols) and Smith (open symbols) force fields for 1,2-dimethoxyethane (circles), 2-methoxyethan-1-ol (squares), 1,2-ethanediol (triangles up), and 1,3-propanediol (triangles down). Experimental data<sup>50,51,61</sup> are shown as lines and stars.

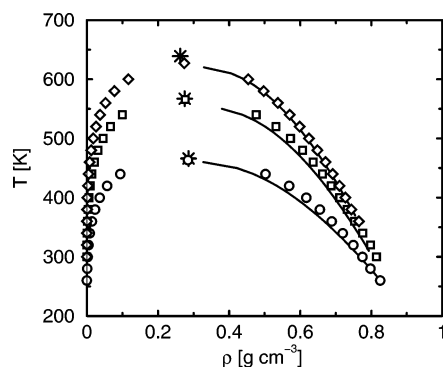


**Figure 9.** Vapor–liquid coexistence curves calculated for the TraPPE–UA force field for acetaldehyde (circles), pentanal (squares), and octanal (diamonds). Solid lines correspond to the correlation of Yaws.<sup>44</sup> Stars represent experimental critical points.<sup>60</sup>

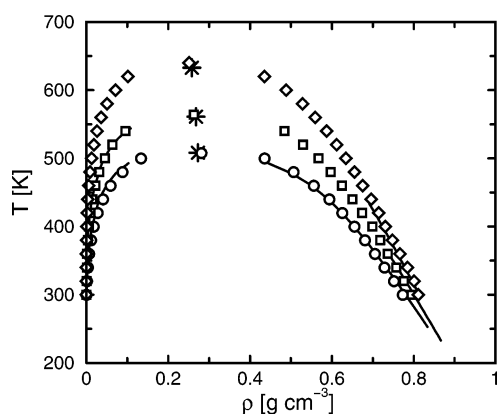


**Figure 10.** Vapor–liquid coexistence curves calculated for the TraPPE–UA force field for acetone (circles), 2-pentanone (squares), and 2-octanone (diamonds). Solid lines correspond to experimental data.<sup>50</sup> Stars represent experimental critical points.<sup>60</sup>

the TraPPE–UA force field predicts saturated liquid densities that are within 1% relative deviation when compared to experiment (ketones)<sup>50</sup> or correlations (aldehydes).<sup>44</sup> The prediction of the critical temperatures is equally robust, with the TraPPE–UA force field yielding values that are within 1% of experiment.

Clausius–Clapeyron plots, used to determine the normal boiling points  $T_b$ , are shown in Figures 11 and 12 for aldehydes and ketones, respectively. The normal boiling points for

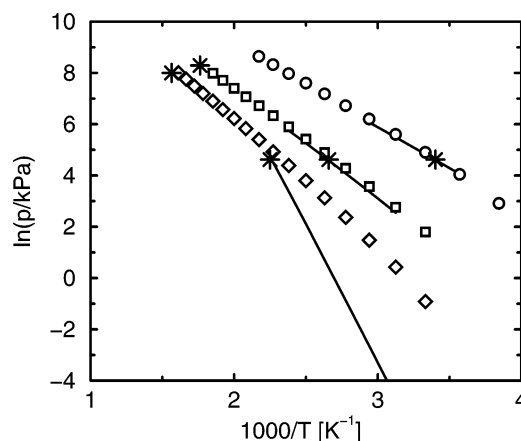


**Figure 11.** Clausius–Clapeyron plots of the saturated vapor pressure versus inverse temperature as predicted by the TraPPE–UA force field for acetaldehyde (circles), pentanal (squares), and octanal (diamonds). Solid lines correspond to the correlation of Yaws,<sup>44</sup> and the stars denote the experimentally determined critical points<sup>60</sup> and normal boiling points.<sup>59</sup>

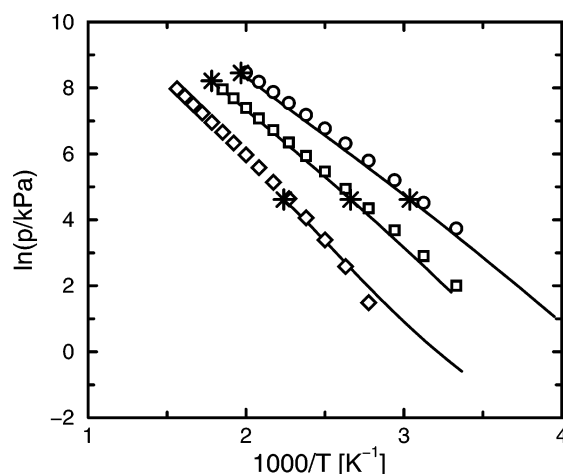


**Figure 12.** Clausius–Clapeyron plots of the saturated vapor pressure versus inverse temperature as predicted by the TraPPE–UA force field for acetone (circles), 2-pentanone (squares), and 2-octanone (diamonds). Solid lines correspond to experimental saturated vapor pressure data,<sup>50</sup> and the stars denote the experimentally determined critical points<sup>60</sup> and normal boiling points.<sup>59</sup>

aldehydes and ketones are listed in Table 4. The largest deviation is found for octanal, where the TraPPE–UA force field predicts  $T_b = 433$  K compared to  $T_b = 444$  K for experiment. For shorter aldehydes, the agreement with experiment is improved. In the case of ketones, the TraPPE–UA force field underpredicts  $T_b$  by about 2% for acetone, and agreement with experiment is somewhat better for 2-pentanone and 2-octanone.

Overall, the vapor pressures for aldehydes and ketones are overpredicted by the TraPPE–UA force field. For the compounds and temperature range investigated here, the maximum relative deviation from experiment of about 20% (overprediction) occurs for octanal. Part of the reason for the discrepancies between experiment and simulation can be traced back to the original parametrization of the  $\text{CH}_3$  and  $\text{CH}_2$  parameters, which resulted in about 10% overprediction of the vapor pressure for  $n$ -alkanes at similar reduced temperatures.<sup>3</sup> In addition to the limits of the united-atom methodology, the accuracy of the force field has been somewhat sacrificed to enforce parameter transferability. The introduction of new parameters for the  $\text{CH}_3$  and  $\text{CH}_2$  pseudo atoms used in this work, fit specifically

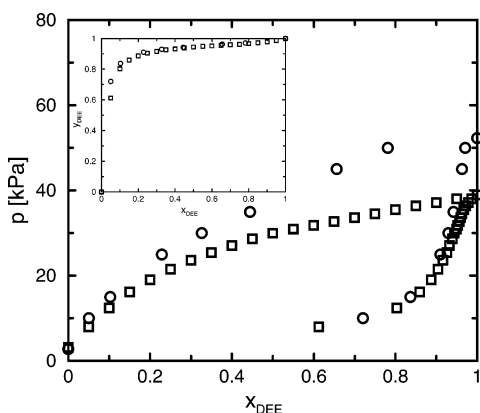


**Figure 13.** Pressure-composition diagram for diethyl ether and ethanol at  $T = 283.15$  K. The squares and circles depict the experimental data<sup>53</sup> and simulation results for the TraPPE-UA force field, respectively. The inset shows the corresponding separation factors.

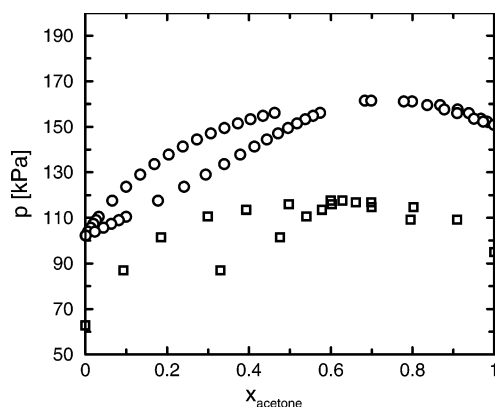


**Figure 14.** Pressure-composition diagram for acetone and hexane at  $T = 328.15$  K. The lines and circles depict the experimental data<sup>52</sup> and simulation results for the TraPPE-UA force field, respectively.

for ketones and aldehydes, is likely to improve the prediction of vapor pressure. The adoption of an explicit hydrogen representation<sup>19</sup> of aldehydes and ketones is also expected to lead to improved predictions of the vapor pressure.

**B. Binary Vapor-Liquid-Phase Equilibria.** The binary VLCC of diethyl ether/ethanol at  $T = 283.15$  K (shown in Figure 13) agrees well with the experimental data points<sup>53</sup> with the majority of error coming from the overestimation of diethyl ether vapor pressures. Furthermore, the separation factors that measure the composition differences of the vapor and liquid phases, are rather well reproduced.

The binary VLCC for the acetone-hexane system at  $T = 328.15$  K is presented in Figure 14. This system consists of a polar (acetone) and nonpolar (*n*-hexane) component with similar vapor pressures. As a result, nonideal, azeotropic behavior is expected, similar to the methanol-hexane system studied in a previous work.<sup>15</sup> Simulations of the TraPPE-UA force fields predict a pressure composition diagram that is in good qualitative agreement with experiment. The positive-pressure azeotrope found in experiment is reproduced by the TraPPE-UA force field, and the predicted azeotropic composition of  $x_{\text{acetone}}^{\text{azeo}} = 0.71$  is in good agreement with the experimental value of  $x_{\text{acetone}}^{\text{azeo}} = 0.64$ .

The overprediction of the azeotropic composition is primarily due to the overprediction of the pure component vapor pressures. Although the vapor pressures for neat *n*-hexane and acetone are overpredicted by approximately 60% (but the absolute shift is larger for acetone), the pressure of the azeotrope is overes-

timated only by 40%. This suggests that unlike-pair interactions between acetone and *n*-hexane are slightly too favorable, which arises primarily from inadequate optimization of the partial charges representing electrostatic interactions. Recent simulations for alkane/ $\text{CO}_2$ <sup>16</sup> and alkene/ $\text{CO}_2$ <sup>54</sup> mixtures have demonstrated that significant improvements in the predictions of mixture phase behavior can be achieved through a relatively simple tuning of the partial charges in addition to Lennard-Jones well depths and size parameters to provide the correct balance of electrostatic and dispersion interactions. Further indication that the strength of the first-order electrostatic interactions (magnitude of the partial charges) are underestimated for acetone comes from its relatively low normal boiling point. A reparametrization of the charges from calculations for binary mixtures will be the focus of future development work in all-atom force fields.

**C. Hydrogen-Bonded Aggregates.** The structure and size distribution of hydrogen-bonded aggregates in the liquid phase were investigated for the pure systems containing diols or glycols and for the binary mixture of diethyl ether and ethanol. For this analysis, only the hydroxyl hydrogen-oxygen acceptor distance was considered when determining the existence of a hydrogen bond because of the differences in the geometries and bond energies of inter- and intramolecular hydrogen bonds that do not allow the application of more commonly employed definitions of multiple geometric and/or energetic criteria.<sup>55</sup> Specifically, in contrast to a previous simulation study by Saiz et al.<sup>56</sup> for 1,2-ethanediol at 298 K and 1 atm, the elevated temperatures investigated here require the additional consideration of intramolecular hydrogen bonds for the liquid phase. For the present study, we decided to analyze hydrogen bonding following a two-step procedure: (i) find the closest oxygen to a given hydroxyl hydrogen and (ii) consider it to form a hydrogen bond with the closest oxygen if the distance is less than 3.3 Å and otherwise to declare the hydroxyl hydrogen to be unbound. The specific cutoff distance of 3.3 Å was chosen because it is the minimum between the first and second peaks in the intramolecular oxygen-hydroxyl hydrogen radial distribution function. Although this cutoff distance alone would be too long for intermolecular hydrogen bonds, overcounting is avoided by restricting hydrogen bonds solely to the nearest oxygen. The application of this simple criterion yields reasonable results for the number of hydrogen bonds per molecule in the liquid phase where the average numbers decrease with increasing temperature: 1.999 at 300 K, 1.983 at 450 K, and 1.845 at 650 K. The low-temperature result compares favorably to the previous simulation estimate of 1.9 intermolecular hydrogen bonds.<sup>56</sup>

A comparison of the intermolecular and total oxygen-hydroxyl hydrogen radial distribution functions for 1,2-ethanediol shows a peak centered at 1.9 Å exclusively due to intermolecular hydrogen bonds, and at higher temperatures, another peak (or shoulder) at about 2.7 Å primarily due to intramolecular hydrogen bonds (Figure 15). The latter peak is attributable to the break up of intermolecular hydrogen bonds at higher temperatures and the formation of additional intramolecular hydrogen bonds. Its peak position coincides with the gas-phase intramolecular hydrogen-bonding peak at  $\sim 2.7$  Å found at all temperatures (not shown). At lower temperature, where fewer intramolecular hydrogen bonds are formed in the liquid (see below), the intramolecular peak is masked by the second-nearest intermolecular oxygen neighbors.

The distributions of interaction energies for pairs of 1,2-ethanediol hydrogen bond donors and acceptors are depicted

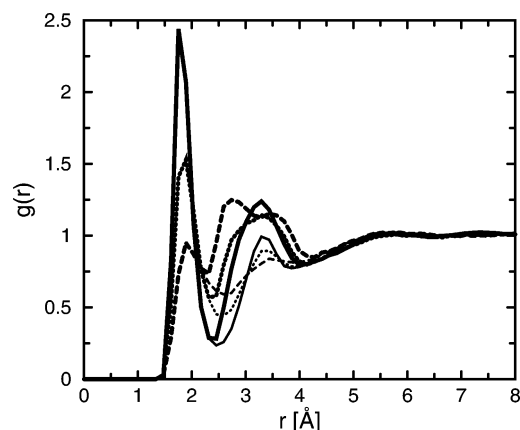


**Figure 15.** Comparison of the intermolecular (thin lines) and total (thick lines) oxygen-hydroxyl hydrogen radial distribution functions for 1,2-ethanediol at  $T = 300$  K (—), 450 K (···) and 650 K (---).

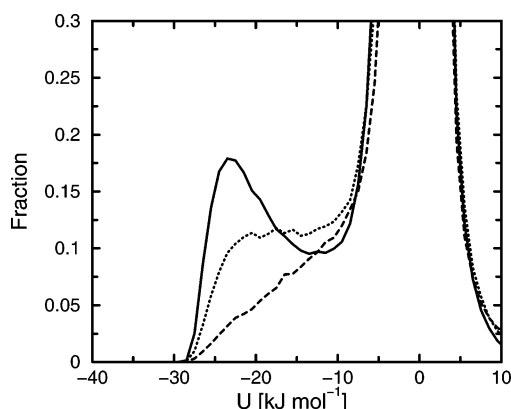


**Figure 16.** Energy distribution of intra- and intermolecular hydroxyl pairs for 1,2-ethanediol at  $T = 300$  K (—), 450 K (···) and 650 K (---).

in Figure 16. The calculation of these pair energies between molecules included the van der Waals and Coulombic contributions as determined by the nonbonded portion of the force field. The calculation of the hydrogen-bond energy within a molecule included all bonded and nonbonded portions of the force field that acted between the donor oxygen and its two bonded neighbors and the acceptor oxygen and its two bonded neighbors (e.g., the full force field for 1,2-ethanediol minus the two H—O—C angle potentials), taken relative to this energy for a conformation of the molecule in which all dihedral angles were trans and all bond angles were at their equilibrium values. The peak centered around  $-23$  kJ mol $^{-1}$  can be attributed to molecules forming an intermolecular hydrogen bond. The intramolecular hydrogen-bonding peak at 450 K was found to be centered around  $-8$  and  $-14$  kJ mol $^{-1}$  in the liquid and gas phases (not shown), respectively. Finally, the main peak located close to  $0$  kJ mol $^{-1}$  is from the majority of disconnected donor/acceptor pairs that are involved in hydrogen bonds with other molecules (not part of the specific pair). The temperature dependence is much stronger in the liquid phase where the hydrogen-bond peaks transform to a shoulder at higher temperatures. The energy difference between a single intramolecular hydrogen bond and a molecular conformation of all-trans dihedral angles compares well with the energy of  $-11.9$  kJ mol $^{-1}$  for the formation of an intramolecular hydrogen bond from an all-trans conformation, as determined from electronic structure calculations in the gas phase.<sup>57</sup>

Figure 17 shows the temperature dependence of the fraction of inter- and intramolecular hydrogen bonds in the liquid phase.

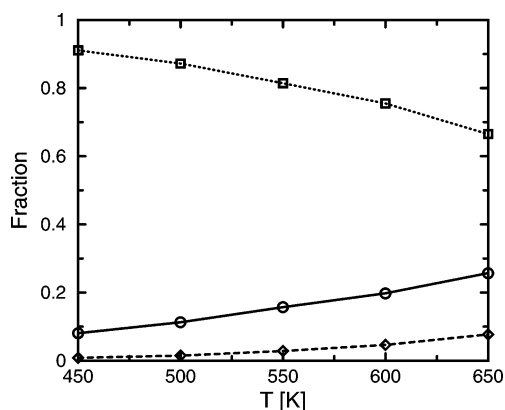


**Figure 17.** Fraction of intra- (—) and intermolecular (···) hydrogen-bonded hydrogens and of free hydrogens (---) in 1,2-ethanediol.

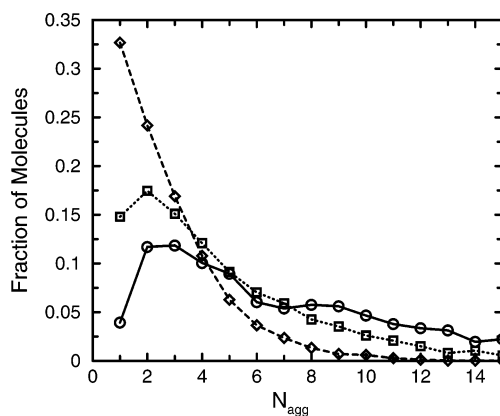
As the temperature increases, the amount of intermolecular hydrogen bonds decreases and the fraction of free (unbound) hydroxyl hydrogens increases (consistent with expectations). However, the amount of intramolecular hydrogen bonding actually increases, despite the fact that intramolecular hydrogen bonds are less favorably formed than their intermolecular counterparts. As the temperature increases (and correspondingly the saturated liquid density decreases), the entropic penalty to form an intermolecular hydrogen bond increases, whereas the energy difference between inter- and intramolecular hydrogen bonds becomes less important.

In contrast to the liquid phase of primary alcohols where the majority of molecules is found in small to mid-size aggregates ( $n < 25$ ),<sup>15</sup> nearly all molecules ( $\sim 200$ ) present in the saturated liquid phases of 1,2-ethanediol belong to the same aggregate. Presumably, the combination of two donor and four acceptor sites per molecule allows for the formation of large percolating clusters.

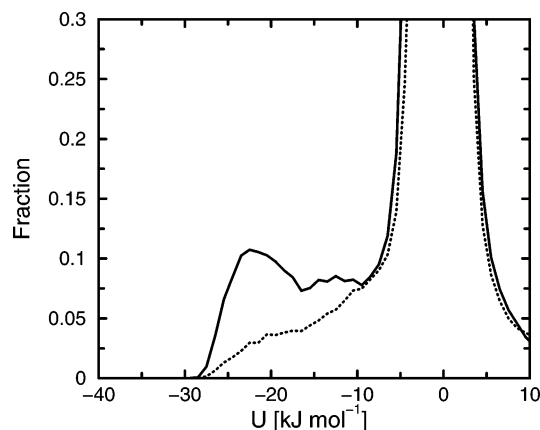
Because 2-methoxyethan-1-ol possesses two distinct acceptor sites (the ether and hydroxyl oxygens), these were treated separately in the analysis of the hydrogen-bonded aggregates. In this case, an interesting observation can be made for the vapor phase; for the lowest number density of 2-methoxyethan-1-ol molecules,  $3.9 \times 10^{-3}$  molecules nm $^{-3}$  (the vapor phase at 347.7 K), the ether acceptor site is preferred, whereas at the slightly higher density of  $2.9 \times 10^{-2}$  molecules nm $^{-3}$  (for the vapor phase at 397.7 K), this preference is reversed and becomes consistent with the liquid-phase results for which the alcohol oxygen is always the preferred acceptor site. This can be attributed to a symmetric dimer bonding structure that allows each molecule to form one hydrogen bond to the other's ether acceptor site, whereas the use of one alcohol acceptor site greatly disfavors the formation of a second hydrogen bond involving the other alcohol acceptor site. Indeed, at 347.7 K, about 20% of the gas-phase dimers sharing two intermolecular hydrogen bonds make use of two ether acceptor sites (with the remaining 80% using one ether and one alcohol acceptor site) and about 60% of the dimers with only one intermolecular hydrogen bond use the hydroxyl acceptor site. However, the formation of an intermolecular hydrogen bond with the ether acceptor sites is energetically less favorable than with the alcohol acceptor sites so that at higher densities where there is competition to form another hydrogen bond to a third molecule the use of the alcohol acceptor site becomes favored.

Figure 18 shows the fraction of 2-methoxyethan-1-ol molecules that were found in a given aggregate size as a function of size for the liquid phase at three different temperatures. At low temperatures, aggregates of sizes 2 and 3 are somewhat





**Figure 18.** Fraction of molecules in aggregates as a function of size for saturated liquid 2-methoxyethan-1-ol at  $T = 347.7$  K (—), 450 K (···) and 550 K (---).



**Figure 19.** Energy distribution of intra- and intermolecular hydroxyl hydrogen-oxygen pairs for 2-methoxyethan-1-ol at  $T = 347.7$  K (—) and 550 K (···).

avored, whereas at higher temperatures, the monomer dominates with a gradual decay in the number of molecules in larger aggregates at increasing aggregate size. The aggregate sizes are relatively small compared to a primary alcohol of similar size (e.g., 1-pentanol) presumably because the formation of intramolecular hydrogen bonds leads to more frequent chain terminations.

Figure 19 depicts the distribution of pair interaction energies for liquid 2-methoxyethan-1-ol at 347.7 and 550 K. Again, the peak associated with the formation of an intermolecular hydrogen bond is located at  $-22$   $\text{kJ mol}^{-1}$ , and the peak height decreases with increasing temperature, similar to 1,2-ethanediol. The intramolecular hydrogen-bond peak is centered around  $-14$   $\text{kJ mol}^{-1}$ . A recent FTIR study<sup>58</sup> investigating the competition between intra- and intermolecular hydrogen bonds for dilute solutions of 2-methoxyethan-1-ol in *n*-hexane at 308 K found the intermolecular hydrogen bond to be 6 times more favorable. This free-energy difference is broadly consistent (after accounting for the different number densities) with the populations of hydrogen-bonded aggregates observed in the gas and liquid phases of this study.

In the case of triethylene glycol, there is competition between the hydroxyl acceptor site and ether acceptor sites along the chain. For a liquid phase at  $T = 310$  K and  $p = 1$  bar, it is found that about 67% of the intermolecular hydrogen bonds involve the energetically favored hydroxyl acceptor site.

Similarly, the formation of hydrogen bonds with a hydroxyl acceptor site is found to be favored in the liquid phase of the binary mixture of diethyl ether and ethanol (Figure 20), which

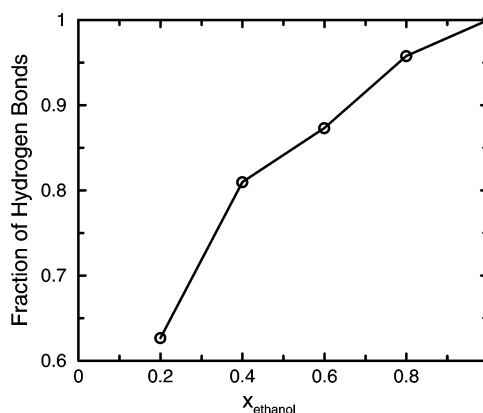


**Figure 20.** Fraction of hydrogen bonds involving a hydroxyl acceptor site observed in the liquid phase of the binary mixture of diethyl ether and ethanol as function of ethanol concentration.

leads to slightly microheterogeneous structure of the liquid, that is, ethanol molecules are preferentially surrounded by other ethanol molecules.

## Conclusion

The TraPPE-UA force field is extended to ethers, glycols, ketones, and aldehydes through the introduction of three new sites, oxygen (ether), carbonyl carbon (ketone) and carbonyl methine (aldehyde), and a special repulsive parameter between a hydroxyl hydrogen and an oxygen belonging to the same molecule but separated by four bonds. Excellent agreement with experimental liquid densities and critical temperatures is achieved, with mean unsigned errors below 1%. The boiling points are found to be underestimated by less than 4%, consistent with earlier results for other molecules in the TraPPE-UA force field. Binary vapor-liquid equilibria for two test systems are in good agreement with experimental results without the need for binary mixing parameters. A detailed analysis of the hydrogen-bonded aggregates in the liquid and vapor phases of 1,2-ethanediol and 2-methoxyethan-1-ol is presented where intermolecular hydrogen bonds are found to dominant for the liquid phases at lower temperatures because they are energetically favored by about 8  $\text{kJ mol}^{-1}$ .

**Acknowledgment.** We thank Bin Chen and Collin Wick for many stimulating discussions. Financial support from the National Science Foundation (CTS-0138393 and CHE-0213387), a Frieda Martha Kunze Fellowship (J.M.S.), a Graduate School Doctoral Dissertation Fellowship (J.M.S.), and a Minnesota Supercomputing Institute Research Scholarship (J.J.P.) are gratefully acknowledged. Part of the computer resources were provided by the Minnesota Supercomputing Institute.

**Supporting Information Available:** The numerical data for the saturated vapor and liquid densities and saturated vapor pressures for neat systems are listed in Tables 5 and 6. The numerical data for the vapor and liquid-phase compositions for the two binary systems are listed in Tables 7 and 8. This material is available free of charge via the Internet at <http://pubs.acs.org>.

## References and Notes

- (1) Briggs, J. M.; Matsui, T.; Jorgensen, W. L. *J. Comput. Chem.* **1990**, *11*, 958.
- (2) Jorgensen, W. L.; Briggs, J. M.; Contreras, M. L. *J. Phys. Chem.* **1990**, *94*, 1683.
- (3) Martin, M. G.; Siepmann, J. I. *J. Phys. Chem. B* **1998**, *102*, 2569.
- (4) Wick, C. D.; Siepmann, J. I.; Schure, M. R. *Anal. Chem.* **2002**, *74*, 37.

- (5) Wick, C. D.; Siepmann, J. I.; Schure, M. R. *Anal. Chem.* **2002**, *74*, 3518.
- (6) Chen, B.; Siepmann, J. I. *J. Phys. Chem. B*, submitted for publication.
- (7) Zaman, M. H.; Shen, M. Y.; Berry, R. S.; Freed, K. F. *J. Phys. Chem. B* **2003**, *107*, 1685.
- (8) Tew, G. N.; Liu, D. H.; Chen, B.; Doerksen, R. J.; Kaplan, J.; Carroll, P. J.; Klein, M. L.; DeGrado, W. L. *Proc. Natl. Acad. Sci. U.S.A.* **2002**, *99*, 5110.
- (9) Heine, D.; Wu, D. T.; Curro, J. G.; Grest, G. S. *J. Chem. Phys.* **2003**, *118*, 914.
- (10) Wick, C. D.; Siepmann, J. I.; Seth, A.; Grant, D. W.; Karaborni, S., to be submitted for publication.
- (11) Kioupis, L. I.; Maginn, E. J. *J. Phys. Chem. B* **1999**, *103*, 10781.
- (12) Kioupis, L. I.; Maginn, E. J. *J. Phys. Chem. B* **2000**, *104*, 7774.
- (13) Moore, J. D.; Cui, S. T.; Cochran, H. D.; Cummings, P. T. *J. Chem. Phys.* **2000**, *113*, 8833.
- (14) Martin, M. G.; Siepmann, J. I. *J. Phys. Chem. B* **1999**, *103*, 4508.
- (15) Chen, B.; Potoff, J. J.; Siepmann, J. I. *J. Phys. Chem. B* **2001**, *105*, 3093.
- (16) Potoff, J. J.; Siepmann, J. I. *AIChE J.* **2001**, *47*, 1676.
- (17) Lorentz, H. A. *Annalen Phys.* **1881**, *12*, 127.
- (18) Berthelot, D. C. R. *Hebd. Seances Acad. Sci.* **1898**, *126*, 1703.
- (19) Chen, B.; Siepmann, J. I. *J. Phys. Chem. B* **1999**, *103*, 5370.
- (20) Wick, C. D.; Martin, M. G.; Siepmann, J. I. *J. Phys. Chem. B* **2000**, *104*, 8008.
- (21) Weiner, S. J.; Kollman, P. A.; Case, D. A.; Singh, U. C.; Ghio, C.; Alagona, G.; Profeta, S., Jr.; Weiner, P. *J. Am. Chem. Soc.* **1984**, *106*, 765.
- (22) Weiner, S. J.; Kollman, P. A.; Nguyen, D. T.; Case, D. A. *J. Comput. Chem.* **1986**, *7*, 230.
- (23) Cornell, W. D.; Cieplak, P.; Bayly, C. I.; Gould, I. R.; Merz, K. M., Jr.; Ferguson, D. M.; Spellmeyer, D. C.; Fox, T.; Caldwell, J. W.; Kollman, P. A. *J. Am. Chem. Soc.* **1995**, *117*, 5179.
- (24) Breneman, C. M.; Wiberg, K. B. *J. Comput. Chem.* **1990**, *11*, 361.
- (25) Frisch, M. J.; Trucks, G. W.; Schlegel, H. B.; Scuseria, G. E.; Robb, M. A.; Cheeseman, J. R.; Zakrzewski, V. G.; Montgomery, J. A., Jr.; Stratmann, R. E.; Burant, J. C.; Dapprich, S.; Millam, J. M.; Daniels, A. D.; Kudin, K. N.; Strain, M. C.; Farkas, O.; Tomasi, J.; Barone, V.; Cossi, M.; Cammi, R.; Mennucci, B.; Pomelli, C.; Adamo, C.; Clifford, S.; Ochterski, J.; Petersson, G. A.; Ayala, P. Y.; Cui, Q.; Morokuma, K.; Malick, D. K.; Rabuck, A. D.; Raghavachari, K.; Foresman, J. B.; Cioslowski, J.; Ortiz, J. V.; Stefanov, B. B.; Liu, G.; Liashenko, A.; Piskorz, P.; Komaromi, I.; Gomperts, R.; Martin, R. L.; Fox, D. J.; Keith, T.; Al-Laham, M. A.; Peng, C. Y.; Nanayakkara, A.; Gonzalez, C.; Challacombe, M.; Gill, P. M. W.; Johnson, B. G.; Chen, W.; Wong, M. W.; Andres, J. L.; Head-Gordon, M.; Replogle, E. S.; Pople, J. A. *Gaussian 98*, revision A.9; Gaussian, Inc.: Pittsburgh, PA, 1998.
- (26) Panagiotopoulos, A. Z. *Mol. Phys.* **1987**, *61*, 813.
- (27) Panagiotopoulos, A. Z.; Quirke, N.; Stapleton, M.; Tildesley, D. J. *Mol. Phys.* **1988**, *63*, 527.
- (28) Smit, B.; de Smedt, P.; Frenkel, D. *Mol. Phys.* **1989**, *68*, 931.
- (29) Ferrenberg, A. M.; Swendsen, R. H. *Phys. Rev. Lett.* **1988**, *61*, 2635.
- (30) Ferrenberg, A. M.; Swendsen, R. H. *Phys. Rev. Lett.* **1989**, *63*, 1195.
- (31) Potoff, J. J.; Panagiotopoulos, A. Z. *J. Chem. Phys.* **1998**, *109*, 10914.
- (32) Siepmann, J. I. *Mol. Phys.* **1990**, *70*, 1145.
- (33) Siepmann, J. I.; Frenkel, D. *Mol. Phys.* **1992**, *75*, 59.
- (34) Frenkel, D.; Mooij, G. C. A. M.; Smit, B. *J. Phys.: Condens. Matter* **1992**, *4*, 3053.
- (35) de Pablo, J. J.; Laso, M.; Suter, U. W. *J. Chem. Phys.* **1992**, *96*, 2395.
- (36) Vlugt, T. J. H.; Martin, M. G.; Smit, B.; Siepmann, J. I.; Krishna, R. *Mol. Phys.* **1998**, *94*, 727.
- (37) Wick, C. D.; Siepmann, J. I. *Macromolecules* **2000**, *33*, 7207.
- (38) Allen, M. P.; Tildesley, D. J. *Computer Simulation of Liquids*; Oxford University Press: New York, 1987.
- (39) Bruce, A. D.; Wilding, N. B. *Phys. Rev. Lett.* **1992**, *68*, 193.
- (40) Wilding, N. B. *Phys. Rev. E* **1995**, *52*, 602.
- (41) Rowlinson, J. S.; Widom, B.; *Molecular Theory of Capillarity*; Oxford University Press: New York, 1989; p 261.
- (42) Rowlinson, J. S.; Swinton, F. L. *Liquids and Liquid Mixtures*, 3rd ed.; Butterworth: London, 1982; pp 70–75.
- (43) Wood, W. W.; Parker, F. R. *J. Chem. Phys.* **1955**, *27*, 720.
- (44) Yaws, C. L. *Thermodynamic and Physical Property Data*; Gulf Publishing Company: Houston, TX, 1992; p 92.
- (45) Timmermans, J. *Physico-Chemical Constants of Pure Organic Compounds*; Elsevier Publishing Company: New York, 1950; p 339.
- (46) Ku, H.-C.; Tu, C.-H. *J. Chem. Eng. Data* **2000**, *45*, 391.
- (47) Smith, G. D.; Jaffe, R. L.; Yoon, D. Y. *J. Phys. Chem.* **1993**, *97*, 12752.
- (48) Smith, G. D.; Yoon, D. Y.; Jaffe, R. L.; Colby, R. H.; Krishnamoorti, R.; Fetters, L. J. *Macromolecules* **1996**, *29*, 3462.
- (49) Watts, L. A. *Fluid Phase Equil.* **2004**, *217*, 37.
- (50) Smith, B. D.; Srivastava, R. *Thermodynamic Data for Pure Compounds: Part A: Hydrocarbons and Ketones*; Elsevier: New York 1986.
- (51) Smith, B. D.; Srivastava, R. *Thermodynamic Data for Pure Compounds: Part B: Halogenated Hydrocarbons and Alcohols*; Elsevier: New York 1986.
- (52) Gmehling, J.; Onken, U.; Arlt, W. *Vapor-Liquid Equilibrium Data Collection*; DECHEMA: Frankfurt, Germany, 1977; p 222–231.
- (53) Ohe, S. *Vapor-Liquid Equilibrium Data*; Elsevier: Tokyo, 1989.
- (54) Weitz, S.; Potoff, J. J., unpublished data.
- (55) Stubbs, J. M.; Siepmann, J. I. *J. Phys. Chem. B* **2002**, *106*, 3968.
- (56) Saiz, L.; Padró, J. A.; Guàrdia, E. *J. Chem. Phys.* **2001**, *114*, 3187.
- (57) Cramer, C. J.; Truhlar, D. G. *J. Am. Chem. Soc.* **1994**, *116*, 3892.
- (58) Brinkley, R. L.; Gupta, R. B. *Ind. Eng. Chem. Res.* **1998**, *37*, 4823.
- (59) Thermodynamics Research Center, NIST Boulder Laboratories, M. Frenkel director, "Thermodynamics Source Database" in NIST Chemistry WebBook, NIST Standard Reference Database Number 69, Linstrom, P. J., Mallard, W. G., Eds., March 2003, National Institute of Standards and Technology: Gaithersburg, MD, 20899 (<http://webbook.nist.gov>).
- (60) Kudchadker, A. P.; Ambrose, D.; Tsonopoulos, C. *J. Chem. Eng. Data* **2001**, *46*, 457.
- (61) Steele, W. V.; Chirico, R. D.; Knipmeyer, S. E.; Nguyen, A.; Smith, N. K. *J. Chem. Eng. Data* **1996**, *41*, 1285.